New Zealand Journal of Marine and Freshwater Research

ISSN: 0028-8330 (Print) 1175-8805 (Online) Journal homepage: www.tandfonline.com/journals/tnzm20

Hydrodynamics of Manukau Harbour, New Zealand

Robert G. Bell, Sergei V. Dumnov, Bryan L. Williams & Malcolm J. N. Greig

To cite this article: Robert G. Bell, Sergei V. Dumnov, Bryan L. Williams & Malcolm J. N. Greig (1998) Hydrodynamics of Manukau Harbour, New Zealand, New Zealand Journal of Marine and Freshwater Research, 32:1, 81-100, DOI: 10.1080/00288330.1998.9516807

To link to this article: https://doi.org/10.1080/00288330.1998.9516807

Published online: 30 Mar 2010.

New Zealand Journal of Marine and Freshwater Research, 1998, Vol. 32: 81–100
0028–8330/98/3201–0081 $7.00/0

Hydrodynamics of Manukau Harbour, New Zealand

ROBERT G. BELL
SERGEI V. DUMNOV[1]
BRYAN L. WILLIAMS[2]
National Institute of Water & Atmospheric Research Ltd
P. O. Box 11 115
Hamilton, New Zealand

MALCOLM J. N. GREIG
National Institute of Water & Atmospheric Research Ltd
P. O. Box 14 901, Kilbirnie
Wellington, New Zealand

[1]Present address: Task Technology Ltd, P. O. Box 68 783, Newton, Auckland, New Zealand.

[2]Present address: Water, Drainage & Refuse Unit, Works & Services Group, Hamilton City Council, Hamilton, New Zealand.

Abstract A calibrated two-dimensional finite-element model, which handles flooding/drying of intertidal areas, complemented by field data, has produced information on tidal propagation in Manukau Harbour, New Zealand with reasonably good accuracy. Excluding the upper-harbour inlets, c. 50% of both the amplification and phase lag in the dominant M_2 tidal constituent occurs through the deep 10-km-long entrance channel to Puponga Point. The calculation of tidal residuals has isolated flood-directed and ebb-directed residual circulation respectively on either side of Puponga Point, which is a typical pattern for alternating flows around headlands. The model has established the dominance of tidal-driven over wind-driven circulation in most of the harbour except in the upper intertidal areas. Wind-driven circulation in the inner Harbour is characterised by downwind flows over intertidal sand banks with pressure-driven return flows (vertically averaged) in the deeper main channels. Tidal dissipation rates are sufficiently high to inhibit the onset of any summer stratification.

Keywords tides; currents; numerical model; residual circulation; winds; estuary; Manukau Harbour

INTRODUCTION

Manukau Harbour is the second largest coastal lagoon on the west coast of the North Island of New Zealand, adjacent to the city of Auckland (Fig. 1). It plays a major role in the coastal ecosystem because of its extensive intertidal sandbanks. It is extensively utilised as a fishery (pelagic and shellfish) and is the recipient of a major treated sewage discharge (mean discharge = 3.9 $m^3 s^{-1}$) from more than 600 000 Auckland residents and associated industries (Vant & Williams 1992).

Over recent years extensive studies of benthic community processes, phytoplankton dynamics, chemistry, and sediment transport within Manukau Harbour have been published (e.g., Pridmore et al. 1990; Vant 1991; Vant & Williams 1992; Thrush et al. 1994; Dolphin et al. 1995; Williamson et al. 1996; Thrush et al. 1997; Green et al. 1997). However, the most recent publication on the physical oceanography of Manukau Harbour, based on limited field measurements, was published 20 years ago (Heath et al. 1977). Increased knowledge of physical processes operating throughout the harbour is needed to elucidate their contributions to *in situ* biological, sedimentological, and chemical variability (both temporal and spatial). Of particular interest are circulation patterns, in both the channels and the extensive intertidal areas (40% of harbour), including the influence of wind. Two previous numerical modelling studies have been undertaken for Manukau Harbour, but with the prime objective to quantify the dispersion of effluent from potential

M97042
Received 6 August 1997; accepted 20 October 1997

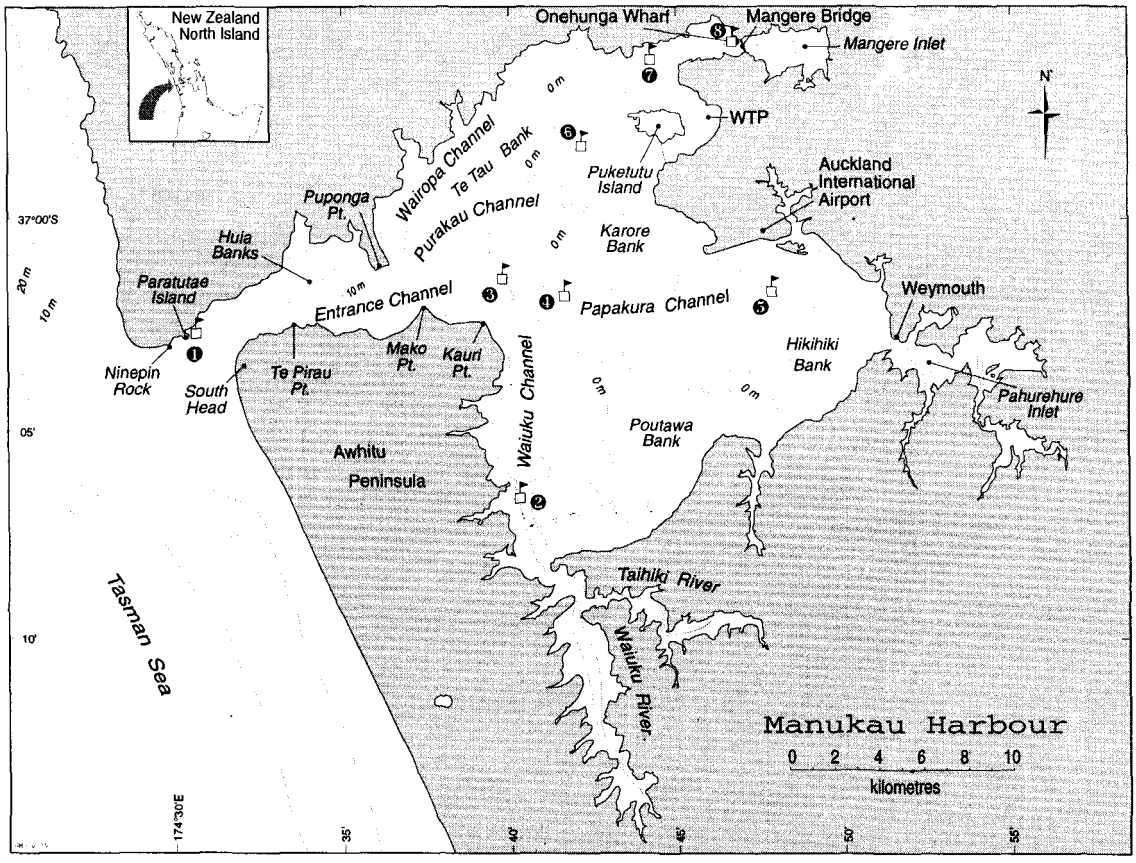

Fig. 1 Location map of Manukau Harbour, New Zealand, showing geographical features, isobaths at 10 m intervals and tidal observation Sites 1–8. (WTP = Mangere Wastewater Treatment Plant.)

discharge sites within the harbour (Delft Hydraulics 1987, 1993a,b; Black et al. 1995, 1996).

This paper describes key features of the tidal and wind-induced circulation within Manukau Harbour, combining results from both a comprehensive field programme and implementation of a hydrodynamic (finite-element) model. The role of the field data was to derive the main tidal harmonic constituents for the harbour and to assist with calibration and verification of the hydrodynamic model. The model provided spatial and temporal information on tides and currents and helped to determine the influence of winds on circulation patterns. The numerical modelling was challenging because finite element models have only recently overcome the difficulties simulating the flooding and drying of intertidal areas (Roig & Evans 1994).

BACKGROUND

Harbour and catchment

Manukau Harbour (Fig. 1) is a large (368 km^2) meso-tidal coastal lagoon which has a sizeable spring tidal prism of 918 3×10^6 m^3 (Heath 1985). The harbour is protected by a large Pleistocene barrier (Awhitu Peninsula) and an extensive ebb-tide delta off the entrance of volume 1250×10^6 m^3 which extends c. 5 km offshore (Hicks & Hume 1996). The basin or inner harbour is connected to the Tasman Sea by a deep (45 m), narrow (2 km wide) entrance channel. Four main channels (Waiuku, Papakura, Purakau, and Wairopa) service the inland tidal inlets (Mangere, Pahurehure, and Waiuku) and streams draining the catchment (Fig. 1).

The surface area, which at mean high water spring tide (368 km^2), is reduced by 60% at low spring tide, with the exposure of broad low-gradient tidal flats and banks covering 145 km^2. Maximum depths across the entrance channel vary from 30 to 50 m in the deepest section off Paratutae Island. Inner-harbour channel depths vary from 30 m at Puponga Point to 5–10 m near the perimeter of the harbour. Minimum depths in the main shoaling sections are: Huia Banks in the entrance channel (5 m), Wairopa Channel (3 m), and Purakau Channel (2.5 m). The volume of the entrance channel at low water is sufficiently large to accommodate the entire tidal prism of the inner harbour (Heath et al. 1976; Vant & Williams 1992).

The catchment area (850 km^2) is only about twice that of the harbour itself, so the mean-annual freshwater inflow (including sewage) of 26.3 $m^3 s^{-1}$ is relatively small (Vant & Williams 1992). This is reflected in the horizontal surface salinity distribution (measured in PSS), routinely monitored around high water, which shows a salinity **difference** between the entrance and the inland tidal inlets of only 4–5 over an average-rainfall year and up to 8 in a very wet season. The water in the harbour can be classified as well mixed, away from the influence of the sewage discharge from the Mangere Wastewater Treatment Plant, with an average salinity increase of only 0.2 down the water column (Vant & Williams 1992; W. N. Vant pers. comm.).

Tides and winds

The tidal ranges in Manukau Harbour are among the highest in New Zealand (Hume et al. 1992). The mean spring (neap) tidal range is amplified inside the harbour, from 2.7 m (1.5 m) at the harbour entrance (Paratutae Island; Fig. 1) to 3.4 m (2.0 m) at Onehunga Wharf in Mangere Inlet (RNZN 1994). Measurements by Heath et al. (1977) showed that peak velocities of up to 1.8 m s^{-1} can occur in the entrance channel. Other regions where high velocities have been measured are in the mouths of the inland tidal inlets: Mangere Inlet, 1.0 m s^{-1} (spring) and 0.5 m s^{-1} (neap) (Hume & Bell 1993; Green & Bell 1994); and Pahurehure Inlet, 0.9 m s^{-1} (neap) (Hume 1979b). Mean tidal excursion distances for the whole harbour were succinctly summarised by harbour box-model segments (Vant & Williams 1992, fig. 1). These tidal excursions are confirmed by drogue tracking data (Heath et al. 1977; Greig & Chiswell 1991). Estimates of the residence times for the upper reaches of the Papakura Channel, Waiuku Channel, and the Wairopa/Purakau system, under mean annual hydrological conditions, are 12, 13, and 26 days respectively (Vant & Williams 1992). More recent work indicates that the residence time for Papakura Channel (i.e., entrance to Pahurehure Inlet), maybe similar to that of the northern channel system.

Prevailing surface-wind directions are from the south-west (average 26% of a year), north to north-east (24%), and west (10%), whereas it is calm for 13% of the time. The median wind speed is c. 6 m s^{-1}. Sustained winds >15 m s^{-1} are seldom experienced (0.2%), usually associated with cold, unstable south-west airstreams (New Zealand Meteorological Service 1982).

METHODS

Field studies

Field studies were concentrated during February–April 1994. Synoptic tidal heights were sampled over c. 1 month at several sites and current velocities at some of these (Fig. 1). Tide height and current measurements from other field studies were also utilised. A summary of instrumentation and deployment information for eight sites is given in Table 1.

Tidal height and current datasets were pre-processed by the removal of glitches and end sections effected by biofouling, then analysed for harmonic constituents using the algorithms of Foreman (1977, 1978). Simultaneous wind velocity and barometric pressure at hourly intervals were obtained from the climate station at Auckland Airport (Fig. 1) to assist with interpretation of water levels and velocities.

Numerical tidal model

The finite-element model RMA-2 (King 1985, 1992; Pierson et al. 1995) was used to simulate the hydrodynamics of Manukau Harbour. This two-dimensional depth-averaged model solves the momentum and continuity equations, treating the two orthogonal velocity components (u, v) and water depth (h) as the dependent variables (King 1992; Roig & King 1992). Boussinesq assumptions are incorporated as eddy viscosity terms to represent turbulent energy losses. Other terms built into the governing equations describe friction losses (approximated by a Chezy formulation), the Coriolis effect, and surface wind stresses. The

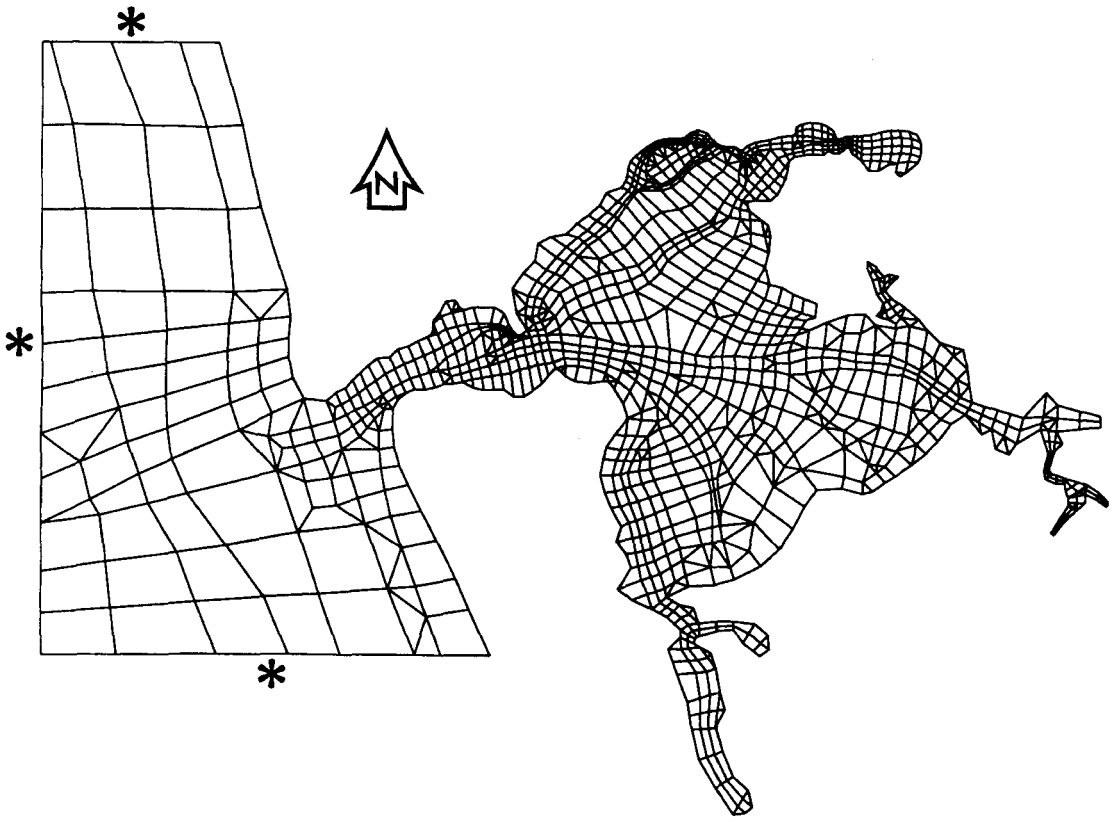

Fig. 2 Finite-element mesh of Manukau Harbour, New Zealand. Asterisks denote where external sea level boundary conditions were applied.

The tide height throughout the model was initially set to a horizontal level at mean sea level (m.s.l.), which is 2.37 m above Chart Datum. A period of 2.5 tidal cycles was allowed for the model to equilibrate. A small model time step of 0.2 h (or 62 time-steps per M_2 tide cycle) was used to ensure accurate system response to the input boundary conditions and minimise truncation errors. Wind effects were simulated by applying surface wind stresses for prevailing south-west and north-east winds, each for two speeds of 7.5 and 15 m s^{-1}. The wind speed was increased gradually from zero to the required value over the equilibration period.

Residual vectors of velocity, shear stress, and dissipation were integrated over a tidal cycle using the Romberg numerical integration technique. For surface-wind simulations, the vector **difference** in residual velocities (wind minus calm) was computed to isolate the component arising solely from the applied wind stress. M_2 tidal amplitudes and phases were computed for all mesh nodes which remained submerged throughout the tidal cycle, using the method described by Foreman & Henry (1989).

Table 2 Sources of bathymetry used to generate the finite-element model mesh.

Harbour region	Bathymetry/shoreline source
Main harbour and coastal region	Chart NZ4314, RNZN (1984); Chart NZ4315, RNZN (1984)
Upper Mangere Inlet	Hume (1979a)
Pahurehure Inlet	NZMS 260, sheet R12; Hume (1979b)
Wiroa Island	Dolphin (1992); T. M. Hume (pers. comm.)
Waiuku River	T. M. Hume (pers. comm.)

RESULTS AND DISCUSSION

Water-surface elevations

Tides

Harmonic analysis of the long-term tidal record from Onehunga Wharf (Site 8; Fig. 1) highlights the dominance of the semi-diurnal (Group 2) tidal constituents, mainly M_2, S_2, and N_2 in descending order (Table 3). These three semi-diurnal constituents account for 97.7% of the variance in the tidal signal compared to 0.2% for the main diurnal constituents (O_1, K_1). For Onehunga Wharf, the tidal form factor F is 0.045, which also classifies the characteristic tide as predominantly semi-diurnal (i.e., F <<0.25; Pugh 1987).

The mean perigean tide range $2(M_2+N_2)$, is slightly less at 3.24 m than the mean spring range, $2(M_2+S_2)$, of 3.42 m. This arises because the solar semi-diurnal tide (S_2) is larger than the elliptical semi-diurnal tide (N_2), in contrast to the east coast of New Zealand (Goring & Bell 1995; Bell & Goring 1996). Therefore the fortnightly spring/neap cycle (following the phases of the Moon) is more pronounced than the monthly perigean/apogean effect (synchronous with the Moon being in its perigee or apogee). Nevertheless with the N_2 amplitude being 75% of the S_2 amplitude, the latter effect is still important in Manukau Harbour, particularly when perigean tides coincide with spring tides every 7.4 anomalistic months (203 days), causing higher than normal spring tides.

Because of the location of Onehunga Wharf in the upper reaches of the harbour, nearly 30 km from the entrance, the tidal record there also exhibits enhanced over-tides (Group 4 and above; Table 3). Over-tides arise in shallow waters as a result of bed-stress non-linearities. The main over-tides at Onehunga Wharf are M_4 (6.2 h) and M_6 (4.1 h) accounting for 0.3% variance. The remaining small variance in the water level record stems from other smaller amplitude Group 2 constituents (e.g., K_2) and low-frequency Group 0 components (Table 3) such as the non-tidal annual cycle (S_a).

The M_2, S_2, and N_2 tidal amplitudes are amplified by 15–21% between the harbour entrance (#1) and the upper reaches of the main channels of the harbour. Phase (time) lags for these same constituents, relative to the harbour entrance, range from c. 40 min to nearly 1 h. In the northern sector, most of this retardation of the tide wave occurs seaward of Site 7 in Wairopa Channel, with only a further 4-min phase lag applying up to Onehunga Wharf (#8). Fig. 3 displays the difference in water levels throughout a spring tidal cycle between the entrance and two upper harbour sites (#5 and #8; Fig. 1). Because of the significant amplification in tidal amplitude between the entrance and Onehunga Wharf, the reduced level of LAT at Paratutae Island is c. 55 cm above LAT or Chart Datum at Onehunga Wharf (D. Hoskins, Ports of Auckland pers. comm.).

Although M_2 dominates non-linear processes during tidal propagation through the harbour basin, its first harmonic (over-tide) M_4, can be used to

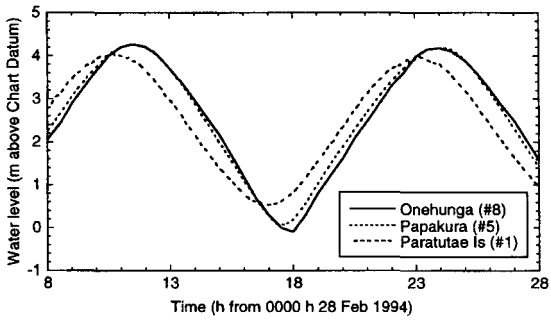

Fig. 3 Comparison of measured spring tide height envelopes for Sites 1 (Paratutae Is.), 5 (Papakura Channel–Wiroa Is.), and 8 (Onehunga Wharf, New Zealand).

Table 3 Main tidal constituents, by frequency groups, computed from harmonic analysis of the long-term tide gauge record for Onehunga Wharf (Site 8, Fig. 1) sourced from Ports of Auckland (unpubl. data), New Zealand. (Phases are relative to the tide-raising force at Greenwich for NZST zone.)

Constituent	Amplitude (cm)	Phase (°)
Group 0 (long period)		
S_a	9.2	26
Group 1 (diurnal)		
O_1	1.7	111
K_1	6.0	208
Group 2 (semi-diurnal)		
N_2	26.9	284
M_2	135.2	301
S_2	35.7	355
K_2	9.8	348
Group 4 (fourth-diurnal)		
M_4	5.5	43
Group 6 (sixth-diurnal)		
M_6	4.2	175

focus on tidal asymmetry in such estuarine systems and their morphological implications (Speer & Aubrey 1985). For the Manukau, the amplitude ratio (M_4/M_2) increases about 4-fold from 0.013 at the entrance to about 0.05 at the upper end of Papakura and Wairopa Channels, with c. 60% of this increase occurring between the entrance and nearest inner-harbour Site 3 (Fig. 1). The relative phase ($2M_2$–M_4) lies in a narrow band, starting at 170° at the entrance (Paratutae Island), rising to a peak of 200° at Sites 2 and 3, then steadily decreases to 180–190° at the upper harbour Sites 5, 8, and 9. These results are discussed later in the context of current patterns.

For eight sites throughout the Harbour (Fig. 1), both observed and modelled M_2 amplitudes (A_o, A_m) and phases (g_o, g_m) are compared in Table 4. The mean difference between modelled and observed amplitude was –1 cm and for phase, 2°. An overall measure of the match between a modelled and observed harmonic constituent is given by the vectorial difference (ΔD) computed as distances in the complex plane (Foreman et al. 1995):

$$\Delta D = \sqrt{(A_o \cos g_o - A_m \cos g_m)^2 + (A_o \sin g_o - A_m \sin g_m)^2} \quad (1)$$

For all sites, $\Delta D \leq 9.5$ cm, with the largest M_2 differences in the upper reaches of Papakura Channel (Sites 4 and 5), whereas in the northern sector of the Manukau, the M_2 tide was more closely matched by the model, with $\Delta D < 4$ cm. The general spatial features of the dominant M_2 tide are shown by the cotidal plots (Fig. 4). The contours have largely been interpolated from the harmonic analysis of model results, but incorporate relevant observed M_2 values where consistent differences from the model occurred, such as the upper Papakura Channel (Table 4). (Note: contours are only approximate for the large intertidal banks.)

The M_2 amplitude attenuates slightly through the harbour entrance (from 111 cm off the ebb-tide delta to 110 cm near Paratutae Island) as the tidal flow is constricted through the narrow entrance (Fig. 4A). Thereafter there is a rapid 10 cm amplification of the M_2 constituent through the deep, narrow entrance channel until it bifurcates into the multiple inner-harbour channels at Puponga Point. Throughout the main inner-harbour basin, another 10–12 cm amplification occurs. Within the southern tidal inlet (Waiuku River), where some observed tidal information is available, the M_2 tide continues to amplify (and slow) moving upstream (Fig. 4) to reach and amplitude of c. 140 cm at the head of the inlet (Tonkin & Taylor 1986). Cophase lines (Fig. 4B) show that about half the total phase lag of the M_2 tidal wave within Manukau Harbour occurs through the confines of the entrance channel, followed by a more slowly varying retardation within the broad, shallower, inner Harbour. The flood-tide delta, Huia Banks (Fig. 1), appears to be the major control on the propagation of the M_2 tidal wave within the entrance channel.

Non-tidal effects

The super-elevation of the mean tide level between the harbour entrance (Paratutae Island) and Onehunga Wharf observed in the M_2 model run was 4.5 cm under calm conditions, which concurs with an estimate of 6 cm derived from survey measurements (Tonkin & Taylor 1986). Super-elevation is caused by the differential celerities of the tidal wave between low and high tides in shallow harbours, requiring a set-up of the half-tide level to redress the imbalance in flow capacity between the wave crest and trough (Ippen 1966; Druery et al. 1983). During persistent wind events, an additional water-surface gradient (set-up or set-down) is generated in Manukau Harbour. Predicted spatial changes in water level arising from either north-east or south-west winds were compared with calm conditions. The greatest differences (set-up or set-down) under windy conditions arise in the shallower inner harbour, rather than in the deeper entrance channel where tidal current velocities are considerably higher. At Onehunga Wharf, during 15-m s^{-1} south-west winds, additional set-ups of 3–4 and 6 cm are predicted by the model for High Water (HW) and Low Water (LW) respectively, whereas for north-east winds at the same speed, set-downs of –3 and –6 cm respectively. The reason for the higher differences at mean LW is that wind-driven set-up varies at any location according to the water depth, with the wind-stress term in the momentum equation depending inversely on the depth of water. During the main field programme the maximum total water-level set-up occurred when a south-west wind peaked at a mean speed of 20 m s^{-1} (21 April 1994). The maximum water level set-up was 45 cm above tidal predictions, comprising wind-stress set-up within the harbour (estimated to be 10+ cm) together with the inverted barometer effect (low atmospheric pressure) and externally-forced coastal set-up.

The annual cycle constituent (S_a) is essentially non-tidal, with the main contributor being the thermo-steric effect on sea level from the seasonal

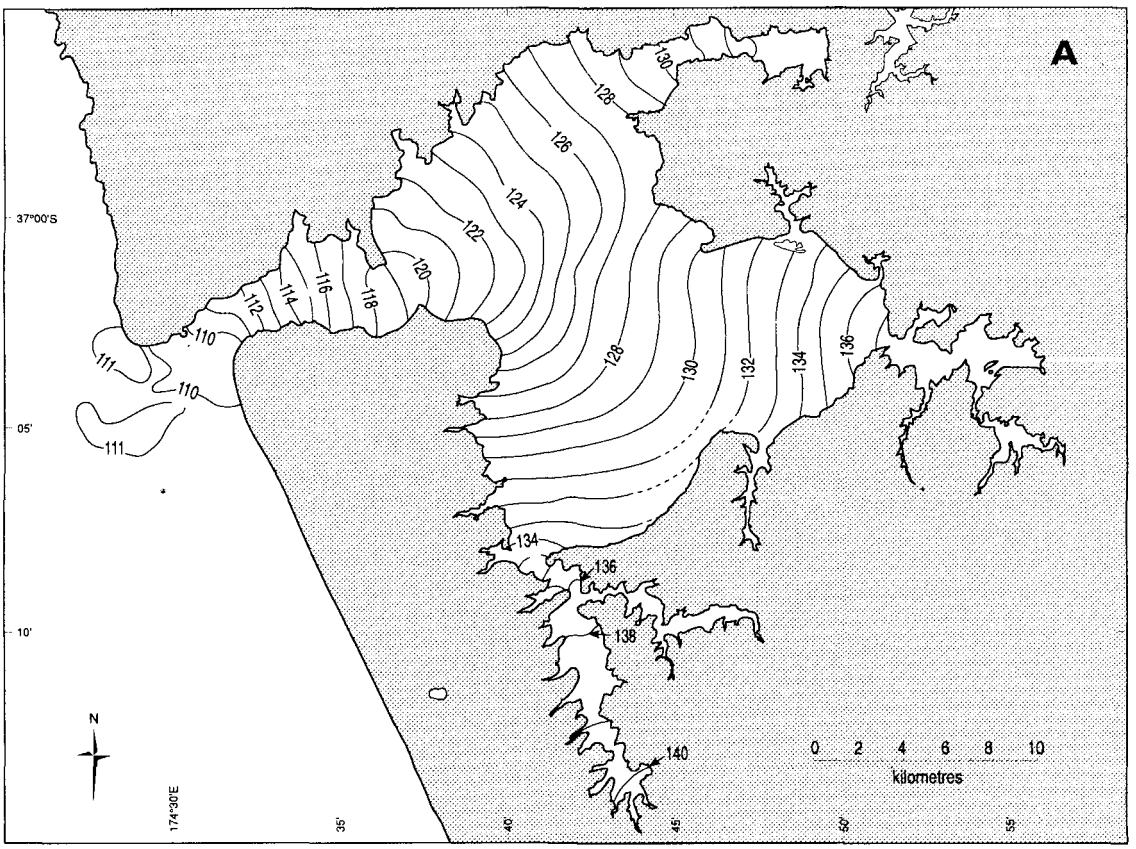

Fig. 4 M_2 cotidal diagrams: **A**, coamplitude (cm); and **B**, cophase (degrees).

heating/cooling cycle (Bell & Goring 1996). This is confirmed by the S_a phase of 26° (Table 3), with the peak height occurring at the end of January (mid summer). The resulting mean S_a amplitude of 9 cm at Onehunga Wharf is somewhat higher than the amplitude of around 5–6 cm obtained from Geosat altimetry for the ocean off the north-west coast of New Zealand (Jacobs et al. 1992). The larger amplitude can be attributed to the greater range of seasonal density variability (water temperature and salinity) and summer evaporation losses within the shallower waters of Manukau Harbour (Vant & Williams 1992).

Table 4 Comparison of observed and modelled M_2 tide-elevation amplitudes (A_o, A_m) and phases (g_o, g_m) for numbered sites shown in Fig. 1 and the vectorial difference D (Equation 1).

	Observed		Model		
Site	A_o (cm)	g_o (°)	A_m (cm)	g_m (°)	ΔD (cm)
1	109.5	280.8	109.8	281.5	1.4
2	131.3	299.5	127.9	302.0	6.6
3	122.1	293.5	123.4	295.8	5.1
4	125.4	293.8	125.5	297.5	8.1
5	132.5	298.8	131.2	302.9	9.5
6	126.0	295.7	126.2	297.5	4.0
7	129.9	299.8	128.0	301.3	3.9
8	132.4	302.4	129.0	302.7	3.5

Currents

Tidal-current characteristics

From the harbour entrance up to the mid-reaches of the main inner-harbour channels (e.g., Sites 2, 5, 7; Fig. 1), the peak current velocities coincide with mid-tide on both flood and ebb. Slack tides throughout the harbour occur within 0–15 min after the respective **local** LW or HW, except the near-shore entrance region off South Head (Fig. 1), where slack tide lags local LW by c. 30 min. The overall

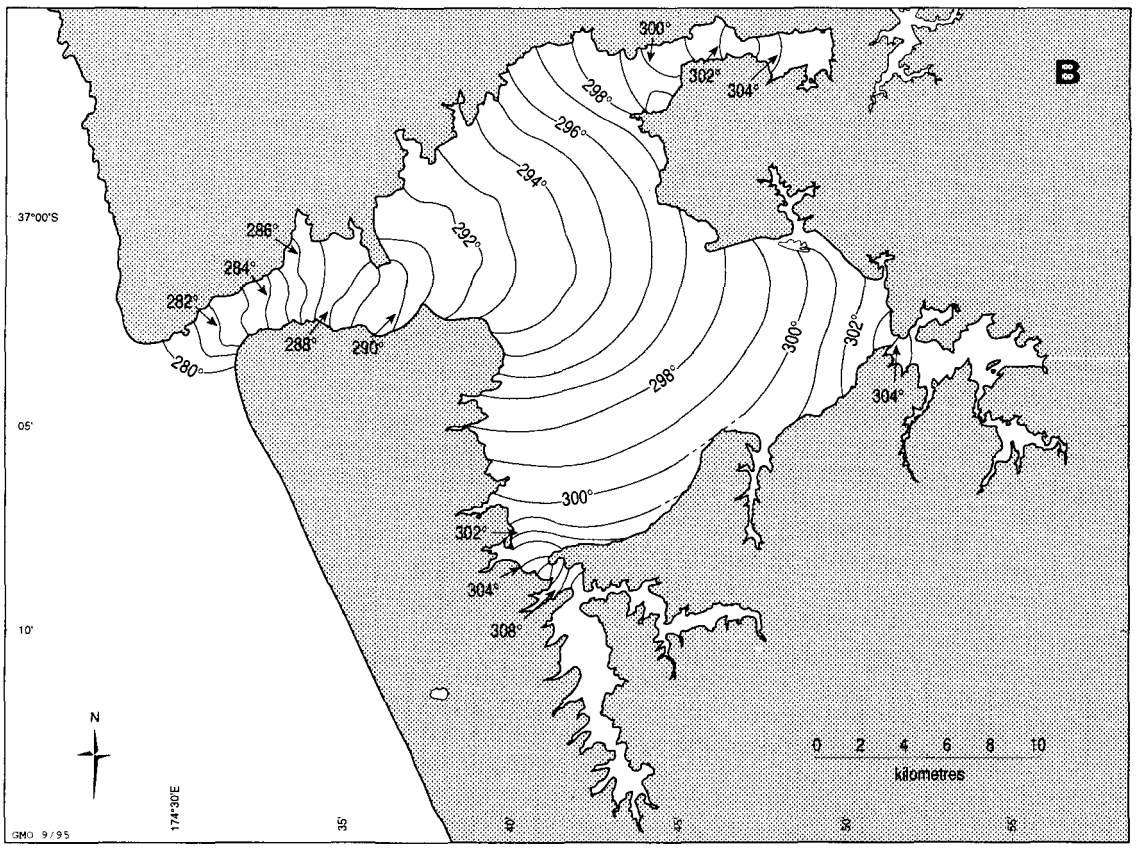

Fig. 4 *(continued)*

phase behaviour characterises the shallow-water tidal wave as a standing wave, as distinct from a progressive wave, and typically occurs in semi-enclosed basins where the tide wave is reflected back on itself (Ippen 1966; Druery et al. 1983). However towards the upper reaches of the harbour, there is a gradual distortion in the velocity phase, with peak currents occurring closer to HW. For example at Onehunga Wharf, the peak-flood velocity is only 1.75 h before HW whereas peak ebb occurs 2.5 h after HW (Hume & Bell 1993; Green & Bell 1994). The M_2 tidal wave in the upper reaches of the Harbour is therefore not strictly a "standing" wave. However with the dominance of friction in such shallow-water systems, both the incident and reflected waves will rarely have similar magnitudes or properties, thus this type of wave classification is suspect (Jay 1991).

Tidal ellipse parameters for various non-overlapping current-meter records of at least 20 days for Papakura and Purakau Channels, are listed in Table 5. Because of the shortness of most records (<28 days), the M_2 amplitudes obtained from harmonic analysis contain a contribution of c. 10% from the unresolved N_2 constituent, which was established from the longer 30-day record at the lower meter in Papakura Channel (#4). Fitting a logarithmic velocity profile to the lower and upper current meter records at Site 4 to derive a depth-averaged M_2 velocity at 0.4 × depth, and incorporating the 10% factor yields a depth-averaged amplitude (major semi-axis) of c. 0.6 m s^{-1} for Papakura Channel, whereas in the smaller Purakau Channel (#6) the depth-averaged M_2 velocity was lower at 0.48 m s^{-1}. Adding S_2 depth-averaged velocities of c. 0.20 and 0.18 m s^{-1} for respective channels yields depth-averaged mean spring-tide velocities of 0.85 m s^{-1} for Papakura Channel (#4) and 0.7 m s^{-1} for Purakau Channel (#6). As expected, the two dominant tidal current

constituents (M_2 and S_2) exhibited strongly rectilinear flow characteristics along the channel axis, shown by the near-zero ellipticity values (Table 5). Strong vertical shear is also evident in the velocity profile at the Papakura Channel site (#4) where the lower meter (0.14 × depth) registered major-axis amplitudes (M_2 and S_2) which were 35% less than the upper meter (0.65 × depth). The inclination of the major tidal axis was found to be nearly constant through the vertical for the dominant M_2 and S_2 components at Site 4, whereas the phases indicate that flow reversal near the bed occurs within a few minutes of that higher in the water column (Table 5).

Tidal circulation

The large tidal range generates strong M_2 tidal currents, particularly in the entrance channel, as shown by the modelled velocity vectors gridded over the harbour (Fig. 5), for mid-flood and mid-ebb relative to the tide state off Puponga Point. Localised maximum **ebb-tide** velocities for a M_2-tide (spring-tide) reached 1.9 m s^{-1} (2.5 m s^{-1}) in the middle of the harbour entrance (Fig. 6B), opposite Ninepin Rock (see Fig. 1), where it begins to shoal towards the offshore delta and 1.7 m s^{-1} (2.2 m s^{-1}) in the southern entrance channel off Te Pirau Point (see Fig. 1), where the ebb-flow is locally constricted by the flood-tide delta (Huia Banks). These peak depth-averaged speeds are comparable to a previous peak spring-tide measurement of 2.25 m s^{-1} at the surface (Heath et al. 1977). Maximum **flood-tide** velocities for M_2-tide (spring-tide) were somewhat lower, reaching 1.5 m s^{-1} (1.8 m s^{-1}) in both the nearshore flood-tide channel off South Head (Fig. 5A, 6D), and off Te Pirau Point (entrance channel). In a transect across the harbour entrance (Ninepin Rock–South Head), peak velocities during the ebb tide exceeded those for the flood tide, except for the southern 20% of the entrance width, where the nearshore flood-tide channel dominates. Further, at this southern end, the flood tide was 1 h longer than the ebb tide, otherwise the durations of both ebb and flood cycles were similar.

Although these results imply that for sediment transport the entrance is ebb-dominated with respect to peak velocities, in terms of the entire harbour, it is only partly consistent with a simplified sedimentary evolutionary sequence for enclosed basins discussed by Lincoln & Fitzgerald (1988) and Speer & Aubrey (1985). Basins such as the Manukau Harbour (a wide drowned river valley), which have been filled with low-lying intertidal banks, but incised with relatively deep channels (M_2 amplitude/depth ratio ≈0.1), possess non-linear hydraulic filling characteristics (water surface area versus tidal elevation) which usually result in an ebb-dominated estuary. However the type of tidal distortion in estuaries (flood-dominant versus ebb-dominant) depends on the relative phasing of the overtide M_4 to M_2 (Speer & Aubrey 1985). Based on tidal elevations discussed earlier, Manukau Harbour exhibits relative phasing in the range

Table 5 Tidal-current ellipse parameters for M_2 and S_2 from mid-channel current-meter deployments (20 days) in Papakura and Purakau Channels, New Zealand. (Ellipticity is the ratio of minor/major semi-axis, phase is relative to maximum ebb velocity, inclination is the orientation of the major axis relative to True North, and Z_0 is the mean residual velocity.)

Site	Height/ water depth (m)	Constituent	Major semi-axis (m s^{-1})	Minor semi-axis (m s^{-1})	Ellipticity	Phase (°)	Inclination (°T)
Papakura Channel							
(#4)	4/28	M_2	0.53	0.01	0.02	37.8	279
		S_2	0.15	0.02	0.13	72.0	277
		Z_0	0.04				303 (ebb)
	18/28	M_2	0.82	0.01	0.01	36.0	278
		S_2	0.23	0.01	0.06	74.0	277
		Z_0	0.02				322 (ebb)
Purakau Channel							
(#6)	7/17	M_2	0.54	–0.01	–0.02	30.1	60
		S_2	0.18	–0.00	–0.01	73.5	63
		Z_0	0.05				69 (flood)

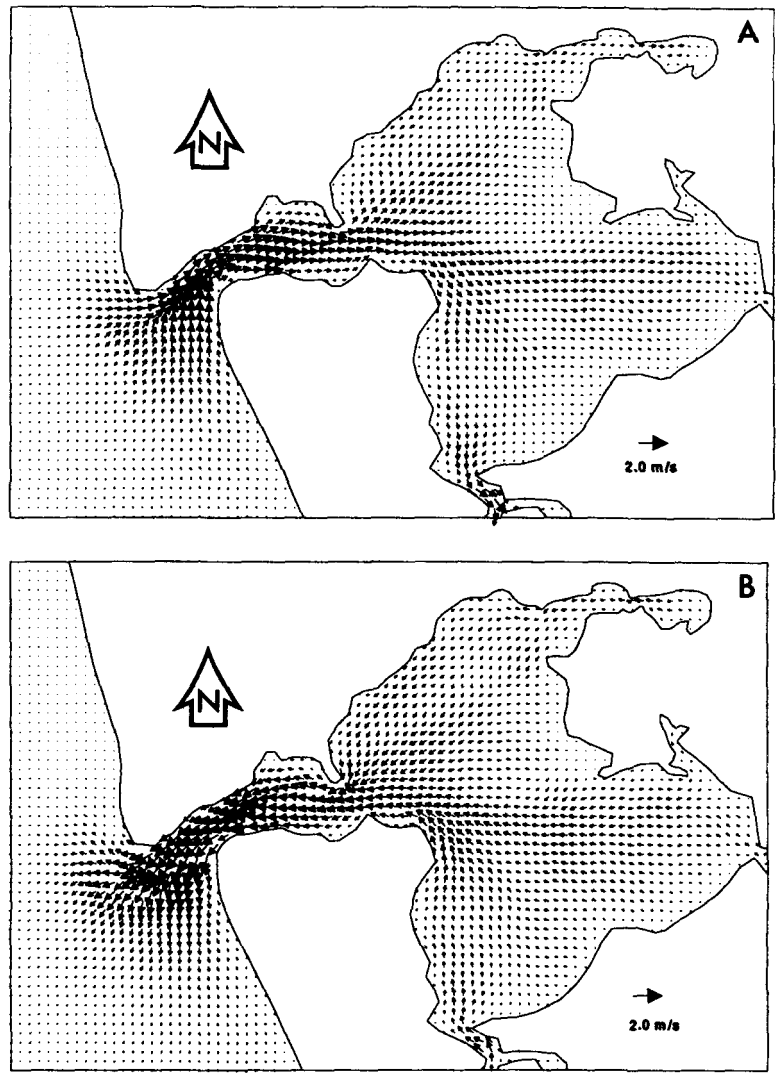

Fig. 5 Modelled M_2 current-vector fields for Manukau Harbour, New Zealand: **A**, peak-flood; and **B**, peak-ebb, relative to tide state in mid-channel off Puponga Point.

170–200°, which straddles the neutral value of 180°, thus not clearly favouring either an ebb-dominated or flood-dominated regime. This neutrality is probably because of the compensatory nature of residual flows in the multiple-branching channels within the Manukau basin, which forms a more complex circulation system than the single main channel assumed by Speer & Aubrey (1985).

The most complex velocity patterns in Manukau Harbour arise in the 9-km-long entrance channel and around Puponga Point headland (Fig. 6), which are strongly influenced by the bathymetry and complex shoreline geometry. Three significant features moderate these complex current patterns: (1) the confluence of the major inner-harbour channels; (2) the constriction imposed by the Puponga Point headland; and (3) the flood-tide delta (Huia Banks) with a minimum water depth of 5 m, which forms a major obstacle to the flow in the middle of the deep entrance channel. A common feature at both HW and LW (Fig. 6A,C) is the early resumption of the next tide phase (flood and ebb respectively) along the nearshore areas on both sides of the entrance channel and the flood-tide channel off South Head in comparison with the mid-channel region and Huia Banks. At both HW and LW,

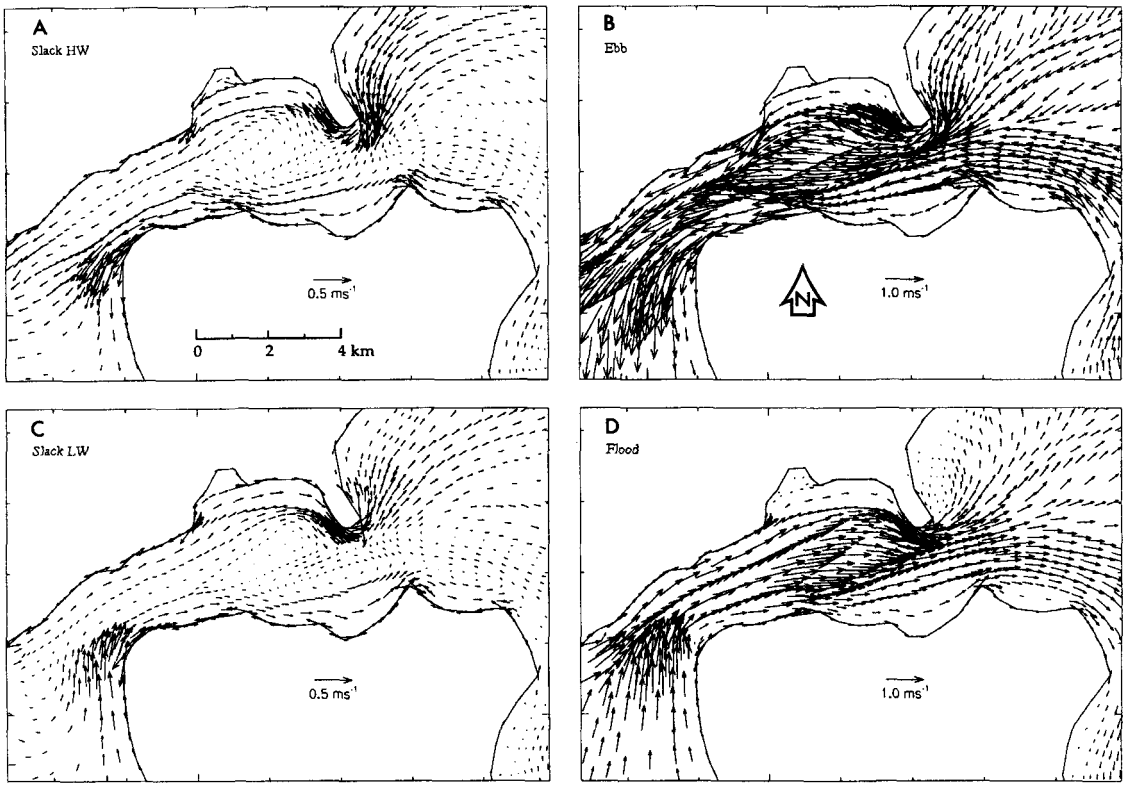

Fig. 6 Modelled M_2 current-vector fields for the Manukau Harbour entrance channel and Puponga Point: **A**, slack high water (HW); **B**, peak-ebb; **C**, slack low water (LW); and **D**, peak-flood. (Note: change of velocity scale for slack-tide plots.)

velocities already have reached 0.5 m s^{-1} in the South Head channel. A small eddy is present between Mako and Kauri Points (Fig. 1), set up by the inertia of the decelerating flow in the large Papakura Channel and the nearshore tidal stream which changes direction earlier. For the peak-ebb tidal stream (Fig. 6B), the majority of streamlines across 75% of the entrance channel off Puponga Point originate from the larger southern basin (Papakura/Waiuku Channels). The remaining streamlines (25% of flow width), which tightly converge around Puponga Point on the northern side, link the northern basin channels to the entrance channel via the northern side of Huia Banks. This modelled behaviour is also confirmed by visual observations, which often show a sharp slick line relatively close to Puponga Point, delineating waters of distinct water clarity originating from southern and northern sectors of the Harbour (W. N. Vant pers. comm.). At peak-flood (Fig. 6D), the flow from the entrance channel north of Huia Banks is again tightly constrained around Puponga Point, but flows mainly into the Purakau Channel. This circulation pattern leaves a weaker flood-tide flow in the northernmost Wairopa Channel, arising from a weak separation eddy in the lee of Puponga Point, which enhances the ebb-dominance of the lower Wairopa Channel. The tightly constrained flow convergence around the Puponga Point headland and, to a lesser extent, around Huia Banks, appears to curtail exchange of water and solutes between the northern and southern channels of the inner harbour as shown by dispersion modelling by Black et al. (1995).

For the inner harbour, peak M_2-tide (spring-tide) velocities > 0.6 m s^{-1} (> 0.8 m s^{-1}) occur in the four main tidal channels (Fig. 5), particularly in the largest channel (Papakura) and at constricted entrances to the inland tidal inlets (Waiuku River, Mangere Inlet, and Pahurehure Inlet). The directions

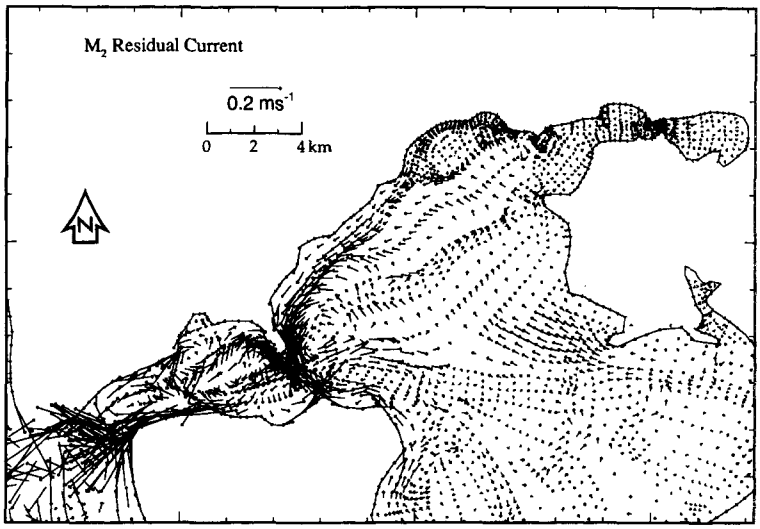

Fig. 7 Modelled M_2 residual currents for Manukau Harbour, New Zealand.

of the tidal currents are generally tangential to the basin isobaths, but because bottom friction strongly affects current speeds, their magnitudes are proportional to mean water depth. Hence currents on the intertidal flats (Fig. 5) are markedly slower than adjacent channels accompanied by a greater tendency for velocities to be directed normal to the isobaths higher up on the flats as they drain or flood (Bell et al. 1997). No large-scale eddies in flow patterns are evident in the inner-harbour because of the relatively narrow, incised, channels. The distance out to the harbour entrance from the both Mangere Inlet (via Wairopa and Purakau Channels) and the outlet from Pahurehure Inlet (via the Papakura Channel), is equivalent to about three tidal excursions on a mean ebb tide (Vant & Williams 1992). Overall, the tidal circulation in Manukau Harbour is primarily governed by volume continuity, where the tidal currents diminish towards the harbour perimeter as both the tidal prism and depths decrease, except at localised inlet constrictions.

Response to wind

Tidal currents in the main channels are not appreciably modified because of either north-east or south-west winds of 15 m s^{-1}, with no discernible change in the deep entrance channel, where current velocities are substantial. The main effect of such wind events is to deviate the current velocities downwind along the shallow, exposed margins of the inner harbour, which is discussed further in the next section. Tide and wind-generated currents in combination with locally generated wind waves, act together to suspend and advect fine sediments from the exposed intertidal banks, leading to enhanced turbidity levels which are a common feature of the water clarity in Manukau Harbour (Vant 1991; Dolphin et al. 1995; Green & Bell 1995; Bell et al. 1997; Green et al. 1997).

Residual currents

Tidal residuals

Figure 7 shows the vector field of the Eulerian tidal residual currents over northern and central sectors of Manukau Harbour, and in Fig. 8, a closer view is presented for the region around Puponga Point. Tidal residual currents are generated by the interaction of tidal currents with bottom topography and harbour geometry and are manifest by ebb tides flowing for different periods than flood tides, differing ebb and flood current magnitudes, or by water masses following different paths. Effective residual mass or solute transport (which includes the covariation of tidal velocity and water depth during a tidal cycle) is enhanced in regions where the Eulerian residual-velocity field is spatially coherent over scales comparable to the tidal excursion. Coherent residual patterns on such scales within the inner-harbour only occur in the Wairopa Channel. Large-scale ebb-directed residual patterns occur in both the lower Wairopa Channel (with moderate residual velocities of up to 0.1 m s^{-1} towards Puponga Point) and along the southern

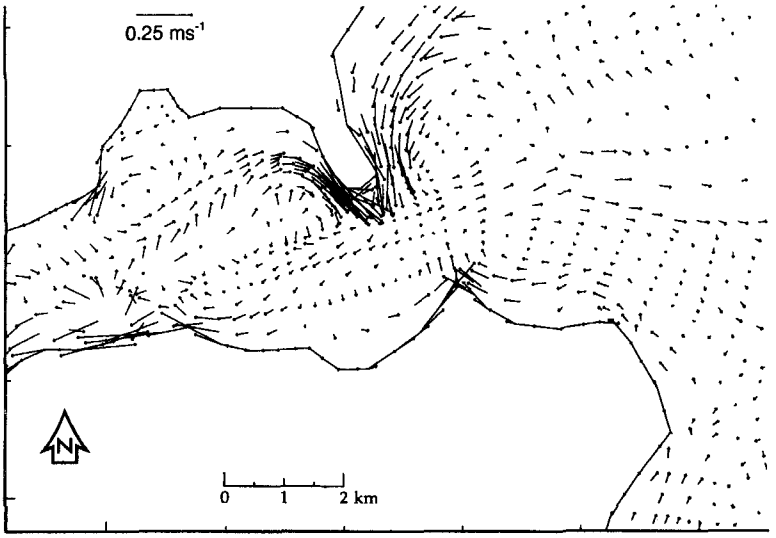

Fig. 8 Modelled M_2 residual current for the Manukau Harbour entrance channel and around Puponga Point headland, New Zealand.

shoreline of the entrance channel from Te Pirau Point through to the entrance (with strong residual velocities of up to 0.35 m s^{-1}), where in both instances these areas are in the lee of the main flood tidal streams. Consistent flood-directed residuals occur along the northern flanks of Huia Banks, continuing on around the seaward side of Puponga Point headland (Fig. 8). The resultant pattern of Eulerian residual velocities generated either side of Puponga Point, and to a smaller extent, Mako Point (Fig. 8), is similar to the residual flow of counter-rotating phase eddies associated with strong oscillatory flows around headlands (Signell & Geyer 1990). However in this instance, development of the eddies is curtailed by the narrow channels and adjacent sandbanks around both sides of the headland compared to the open coast situation (Hume et al. 1997).

The residual flow pattern immediately seaward of Manukau Harbour entrance is typical of ebb-tide deltas (Oertel 1988), where sediments are expelled through an ebb-dominated flow through the central region of the delta, whereas a flood-dominated flow occurs along the nearshore zones of the coastal barriers. However as a consequence of the offset coastal barriers either side of the entrance, the flood tidal stream is strongest through the nearshore flood-channel off South Head (Fig. 6D).

Steady-state wind response

The response of residual currents in Manukau Harbour to steady-state winds was examined for prevailing south-west and north-east winds of 7.5 and 15 m s^{-1} and compared with calm conditions. Vector differences in depth-averaged Eulerian residuals (wind minus calm) from the model results (Fig. 9), show the depth-averaged wind-induced circulation in the north-east sector of the Harbour. The wind-driven motion for the two north-east wind scenarios are shown in Fig. 9A,B and similarly for south-west winds in Fig. 9C,D. The first noticeable feature of the results is the non-linear response to increasing wind speed, where the wind-induced flows are markedly higher (more than 2×) for 15 m s^{-1} winds, represented by the wind-stress term which is quadratic in wind speed. Second, the greatest wind response occurs on the shallow intertidal flats, rather than in the channels, arising from the inverse-depth relationship in the wind-stress term.

During **north-east** winds (Fig. 9A,B), consistent downwind flows occur along the entire north-eastern perimeter, commencing inside Mangere Inlet. A westerly-directed flow off Wiroa Island and past the Airport on the northern side of Papakura Channel merges with the residual flow along the north-eastern perimeter. Downwind wind-induced flows also occur along the entire length of Te Tau Bank and along the northern branch of Wairopa Channel, where it shoals. As discussed previously, the set-down in water elevations in the eastern sector of the harbour, arising from a north-east wind, creates water-surface gradients which drive residual vertically-integrated counter-flows upwind in the

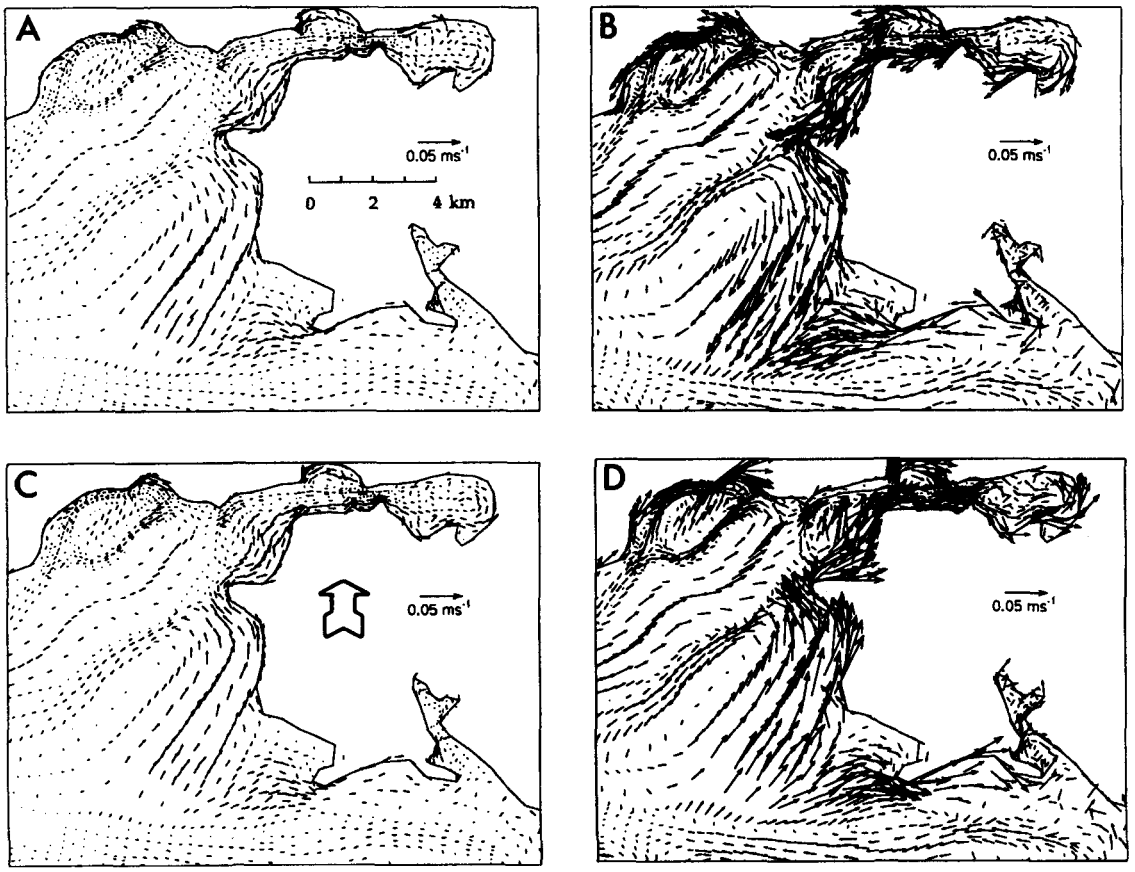

Fig. 9 Wind-induced residual circulation for the north-east sector of Manukau Harbour, New Zealand for—north-east winds: **A**, 7.5 m s^{-1}; and **B**, 15 m s^{-1}; and south-west winds: **C**, 7.5 m s^{-1}; and **D**, 15 m s^{-1}.

main channels, as shown in Fig. 9B, although in the surface layer, residual flows may well be downwind. In particular, the total flood-directed residual flow in Purakau Channel (south-west of the Mangere WTP) is virtually doubled to 0.05 m s^{-1} with the addition of the wind-induced counter-flow from a 15-m s^{-1} north-east wind. The wide southern intertidal banks (Poutawa and Hikihiki) are the only other areas where pronounced wind-driven flows occur, up to 0.1 m s^{-1} downwind.

For prevailing **south-west** winds (Fig. 9C,D), the wind-induced circulation exhibits similar magnitudes, but reversed, to the pattern which occurs during equivalent-speed north-east winds. This implies a near-linear response of the Manukau Harbour basin to wind-forcing of equal magnitude from the two dominant wind directions. During south-westerlies, a coherent north to north-east wind-induced flow is established at higher tide levels along the north-eastern perimeter through to Mangere Inlet. This mechanism partly explains the large influx of suspended sediment measured by Green & Bell (1995) on the southern side of Mangere Inlet during the late stages of a flood tide, after a persistent south-west breeze of 6–8 m s^{-1}, together with locally-sourced sediment stirred from the adjacent nearshore surf zone. Wind-induced flows (depth-averaged) in the main channels are upwind, which is to the south-west in the instance of lower Purakau Channel, virtually cancelling out the tidal residual current.

Thus, the wind-driven circulation in Manukau Harbour is characterised by downwind-directed flows on the shallow intertidal sand banks with pressure-driven return flows (vertically-averaged) in the deeper main channels of the inner harbour.

This same pattern was demonstrated by Glorioso & Davies (1995) using a three-dimensional model for an estuary with a deep central channel flanked by shallow areas. In these instances for well-mixed estuaries, the circulation and flushing time are determined largely by horizontal processes and, hence, are fairly insensitive to the magnitude of the vertical eddy viscosity. As expected, the wind effect on depth-averaged flows in the deep entrance channel is negligible, although surface currents may be significantly affected by strong winds.

Bottom stress, dissipation rate and tidal stirring

The mean bottom frictional stress (τ_β) during a tidal cycle T (Bowman et al. 1980), which is of interest in sediment transport, is given by:

$$\tau_\beta = \frac{1}{T}\int_0^T \frac{\rho g}{C^2}|\tilde{U}|^2 \, dt \qquad (2)$$

where ρ = density of sea water, assumed constant; g = acceleration as a result of gravity; and $\tilde{U}$ is the depth-averaged current velocity. As expected from the current velocities, the regions of highest bottom stress are located in the entrance (off Ninepin Rock) and along the southern side of the entrance channel seaward of Te Pirau Point, with a maximum value of 3.6 N m^{-2} in the entrance. Mean bottom stresses above 0.1 N m^{-2} occur in the western half of the harbour (seaward of the 174° 41′ E meridian), plus the entrance to Waiuku River tidal inlet. Low tidal bottom stresses (< 0.01 N m^{-2}) occur over the intertidal flats arising from both relatively low velocities and shorter inundation periods, but conversely bottom stresses generated by wind-waves are much higher in these shallow areas causing high turbidities (Bell et al. 1997; Green et al. 1997). The dissipation rate of M_2 energy by bottom friction, which represents the rate of work per unit area made by the water column against bottom friction (where the current velocity in Equation 2 is cubed; Bowman et al. 1980), is similar to the bottom stress distribution. High dissipation rates (> 0.05 W m^{-2}) occur in the entrance channel (maximum off Ninepin Rock of 5.3 W m^{-2}) and the seaward ends of the inner-harbour channels. As an indication of the ability of vertical tidal stirring to inhibit summer stratification, Simpson & Hunter (1974) derived a stratification index (h/u^3), where at any location, h is the water depth, and u is the amplitude of the mean-spring tidal current. Low values indicate areas which remain well mixed vertically. Intermediate values in the range 30–100 up to 500 m^{-2} s^3 (Simpson & Hunter 1974; Bowman et al. 1980; Argote et al. 1995) have been associated with frontal structures found in shelf seas and produced by variations in tidal mixing. Values of this index in the entrance to Manukau Harbour are low (< 5 m^{-2} s^3) as expected, because of high tidal dissipation rates. For the main channels dissecting the inner Harbour, the stratification index is mainly in the range 20–35 m^{-2} s^3. Therefore summer stratification is unlikely, as confirmed by regular water-column observations.

CONCLUSIONS

A two-dimensional finite-element model, which handles flooding/drying of intertidal areas, complemented by field data, has produced information on tidal propagation in Manukau Harbour with reasonably good accuracy. Excluding the upper-harbour inlets, c. 50% of both the amplification and phase lag in the dominant M_2 constituent occurs through the deep 10-km-long entrance channel to Puponga Point. The calculation of tidal residuals has isolated flood-directed and ebb-directed residual circulation respectively on either side of Puponga Point, which is a typical pattern for alternating flows around headlands. The model has established the dominance of tidal-driven over wind-driven circulation in most of the harbour except higher up on the intertidal areas. Wind-driven circulation in the inner harbour is characterised by downwind flows over intertidal sand banks with pressure-driven return flows (vertically-averaged) in the deeper main channels. Tidal dissipation rates are sufficiently high to inhibit the onset of any summer stratification.

ACKNOWLEDGMENTS

Thanks to: Rod Budd, John Nagels, and Tony Dolphin for field assistance; Auckland Regional Council for granting permission to use Papakura and Purakau Channel current-meter data; Dave Hoskins (Ports of Auckland) for supplying Onehunga Wharf tide data and datum information; and Roy Walters (USGS, Tacoma), Ian King (University of California, Davis), and Falconer Henry (Institute of Ocean Sciences, Victoria BC) for helpful advice on modelling and grid generation. Reviews by Kerry Black, Terry Hume, Graham McBride, and Bill Vant provided many useful suggestions. This study was funded by the N.Z. Foundation for Research, Science and Technology (Contract CO1211).

REFERENCES

Argote, M. L.; Amador, A.; Lavín, M. F.; Hunter, J. R. 1995: Tidal dissipation and stratification in the Gulf of California. *Journal of geophysical research 100(C8)*: 16103–16118.

Bell, R. G.; Goring, D. G. 1996: Techniques for analyzing sea level records around New Zealand. *Marine geodesy 19(1)*: 77–98.

Bell, R. G.; Hume, T. M.; Dolphin, T. J.; Green, M. O.; Walters, R. A. 1997: Characterisation of physical environmental factors on an intertidal sandflat, Manukau Harbour, New Zealand. *Journal of experimental marine biology and ecology 216(1–2)*: 11–31.

Black, K. P.; Bell, R. G.; Oldman, J. W.; Gorman, R. M. 1996: Challenges encountered modelling a diffuse shoreline discharge from the Mangere WTP. *In*: Striking the balance, Proceedings of NZWWA Annual Conference, Nelson. Auckland, NZ Water & Wastes Association. Pp. 264–268.

Black, K. P.; Bell, R. G.; Oldman, J. W.; Gorman, R. M.; Oulton, D. 1995: Numerical modelling of a future diffuse shoreline discharge option for the Mangere Wastewater Treatment Plant. Report for Watercare Services Ltd, Auckland. NIWA Consultancy Report. 106 p.

Bowman, M. J.; Kibblewhite, A. C.; Ash, D. E. 1980: M_2 tidal effects in greater Cook Strait, New Zealand. *Journal of geophysical research 85(C5)*: 2728–2742.

Delft Hydraulics 1987: Auckland area sewerage study. Manukau Harbour dispersion modelling. *Report Z226*. A report to the Auckland Regional Authority. 46 p.

Delft Hydraulics 1993a: Manukau Harbour dispersion modelling. Part I. Preparation and verification of existing hydrodynamic model. *Report Z472*. A report to Watercare Services Ltd, Auckland. 7 p.

Delft Hydraulics 1993b: Manukau Harbour dispersion modelling, Auckland, New Zealand. Part II. Refinement and recalibration of hydrodynamic model: water quality simulations. *Report Z472*. A report to Watercare Services Ltd, Auckland. 30 p.

Dolphin, T. J.; Hume, T. M.; Parnell, K. E. 1995: Oceanographic processes and sediment mixing on a sand flat in an enclosed sea, Manukau Harbour, New Zealand. *Marine geology 128*: 169–181.

Dronkers, J. J. 1964: Tidal computations in rivers and coastal waters. Amsterdam, North-Holland Publishing Co. 518 p.

Druery, B. M.; Dyson, A. R.; Greentree, G. S. 1983: Fundamentals of tidal propagation in estuaries. *In*: Proceedings of 6th Australasian Conference on Coastal and Ocean Engineering, Gold Coast. Canberra, The Institution of Engineers—Australia. Pp.187–193.

Egbert, G. D.; Bennett, A. F.; Foreman, M. G. G. 1994: TOPEX/POSEIDON tides estimated using a global inverse model. *Journal of geophysical research 99(C12)*: 24821–24852.

Foreman, M. G. G. 1977: Manual for tidal heights analysis and prediction. *Pacific marine science report 77–10*, Institute of Ocean Sciences, Patricia Bay, Victoria, British Columbia, Canada. 101 p.

Foreman, M. G. G. 1978: Manual for tidal currents and prediction. *Pacific marine science report 78–6*, Institute of Ocean Sciences, Patricia Bay, Victoria, British Columbia, Canada. 70 p.

Foreman, M. G. G.; Henry, R. F. 1989: The harmonic analysis of tidal model time series. *Advances in water resources 12*: 109–120.

Foreman, M. G. G.; Walters, R. A. 1990: A finite-element tidal model for the southwest coast of Vancouver Island. *Atmosphere-ocean 28*: 261–287.

Foreman, M. G. G.; Walters, R. A.; Henry, R. F.; Keller, C. P.; Dolling, A. G. 1995: A tidal model for eastern Juan de Fuca Strait and the southern Strait of Georgia. *Journal of geophysical research 100(C1)*: 721–740.

Glorioso, P. D.; Davies, A. M. 1995: The influence of eddy viscosity formulation, bottom topography, and wind wave effects upon the circulation of a shallow bay. *Journal of physical oceanography 25*: 1243–1264.

Goring, D. G.; Bell, R. G. 1995: Variation of sea level on the Canterbury coast of New Zealand. *In*: Proceedings of 12th Australasian Conference on Coastal and Ocean Engineering, Melbourne. *National conference publication 95/5*. Canberra, The Institution of Engineers—Australia. Pp. 275–278.

Green, M. O.; Bell, R. G. 1994: Field studies of tidal flows and suspended distributions in Mangere Inlet. *NIWA Internal report IR94/03*. Hamilton, NIWA. 42 p.

Green, M. O.; Bell, R. G. 1995: Wave influence on suspended-sediment fluxes in an estuary (Manukau Harbour, New Zealand). *In*: Proceedings of 12th Australasian Conference on Coastal & Ocean Engineering, Melbourne. *National conference publication 95/5*. Canberra, The Institution of Engineers—Australia. Pp. 59–64.

Green, M. O.; Black, K. P.; Amos, C. L. 1997: Control of estuarine sediment dynamics by interactions between currents and waves at several scales. *Marine geology 144*: 97–116.

Greig, M. J.; Chiswell, S. M. 1991: Hydrological Investigations Manukau Harbour. Report on first stage investigations. Papakura Channel. *Report no. 1991/5(3)*, New Zealand Oceanographic Institute, DSIR Marine and Freshwater, Wellington (now NIWA). A report to the Auckland Regional Council. 17 p.

Greig, M. J.; Stanton, B. R. 1992: Hydrological Investigations Manukau Harbour. Report on currents in Purakau Channel, Manukau Harbour. *Report no. 1992/20*, New Zealand Oceanographic Institute, DSIR Marine and Freshwater, Wellington (now NIWA). A report to the Auckland Regional Council. 4 p.

Heath, R. A. 1985: A review of the physical oceanography of the seas around New Zealand—1982. *New Zealand journal of marine and freshwater research 19*: 79–124.

Heath, R. A.; Greig, M. J. N.; Shakespeare, B. S. 1977: Circulation and hydrology of Manukau Harbour. *New Zealand journal of marine and freshwater research 11*: 589–607.

Hicks, D. M.; Hume, T. M. 1996: Morphology and size of ebb tidal deltas at natural inlets on open-sea and pocket-bay coasts, North Island, New Zealand. *Journal of coastal research 12*: 47–63.

Hume, T. M. 1979a: Aspects of the hydrology of the Mangere Inlet–Wairopa Channel area, northeast Manukau Harbour. Auckland, Water and Soil Division, Ministry of Works and Development. 62 p.

Hume, T. M. 1979b: Tidal observations in Pahurehure Inlet, Manukau Harbour. Auckland, Water and Soil Division, Ministry of Works and Development. 16 p.

Hume, T. M.; Bell, R. G. 1993: Methods for determining tidal flows and material fluxes in estuarine cross-sections. Hamilton, New Zealand, *Water Quality Centre publication 22*, DSIR Marine and Freshwater (now NIWA). 57 p.

Hume, T. M.; Bell, R. G.; de Lange, W. P.; Healy, T. R.; Hicks, D. M.; Kirk, R. M. 1992: Coastal oceanography and sedimentology in New Zealand, 1967–91. *New Zealand journal of marine and freshwater research 26*: 1–36.

Hume, T. M.; Oldman; J.W.; Black, K. P. 1997: Signatures of wave and current forcing on the seabed about a large coastal headland. *In*: Pacific Coasts and Ports '97, Proceedings of 13th Australasian Conference on Coastal and Ocean Engineering, Christchurch. Christchurch, Centre for Advanced Engineering. Pp. 319–324.

Ippen, A. T. 1966: Estuary and coastline hydrodynamics. New York, McGraw Hill Co. 744 p.

Jacobs, G. A.; Born, G. H.; Parke, M. E.; Allen, P. C. 1992: The global structure of the annual and semiannual sea surface height variability from Geosat altimeter data. *Journal of geophysical research 97(C11)*: 17813–17828.

Jay, D. A. 1991: Green's law revisited: tidal long-wave propagation in channels with strong topography. *Journal of geophysical research 96(C11)*: 20585–20598.

King, I. P. 1985: Strategies for finite element modeling of three dimensional hydrodynamic systems. *Advances in water resources 8*: 69–76.

King, I. P. 1992: Evaluation of modelling parameters for simulation of estuarial systems. *In*: Spaulding, M. L.; Bedford, K.; Blumberg, A.; Cheng R.; Swanson, C. *ed.* Estuarine and coastal modeling. Proceedings of the 2nd International Conference, Tampa, Florida. New York, ASCE. Pp. 707–719.

King, I. P. 1994: RMAGEN—a program for generation of finite element networks. Version 3.3(a), User manual. Davis, University of California. 21 p.

Lincoln, J. M.; Fitzgerald, D. M. 1988: Tidal distortions and flood dominance at five small tidal inlets in Southern Maine. *Marine geology 82*: 133–148.

New Zealand Meteorological Service 1982: The climatology of Auckland International Airport (1965–1978). *Miscellaneous publication 171(2)*. 20 p.

Oertel, G. F. 1988: Processes of sediment exchange between tidal inlets, ebb deltas and barrier islands. *In*: Aubrey, D. G.; Weishar, L. *ed.* Hydrodynamics and sediment dynamics of tidal inlets. *Lecture notes on coastal and estuarine studies 29*. New York, Springer-Verlag. Pp. 297–318.

Pierson, W. L.; Roizenblit, A.; Wang, Y. C. 1995: Numerical modelling of pollutant transport processes in Bate Bay, New South Wales. *In*: Proceedings of 12th Australasian Coastal & Ocean Engineering Conference, Melbourne. *National conference publication 95/5*. Canberra, The Institution of Engineers—Australia. Pp. 139–144.

Pridmore, R. D.; Thrush, S. F.; Hewitt, J. E.; Roper, D. S. 1990: Macrobenthic community composition of six intertidal sandflats in Manukau Harbour, New Zealand. *New Zealand journal of marine and freshwater research 24*: 8196.

Pugh, D. T. 1987: Tides, surges and mean sea-level. A handbook for engineers and scientists. Chichester, John Wiley and Sons. 472 p.

RNZN 1994: New Zealand nautical almanac 1995. *Publication NZ 204*. Auckland, Hydrographic Office of the Royal New Zealand Navy. 192 p.

Roig, L. C.; Evans, R. A. 1994: Environmental modeling of coastal wetland. *In*: Spaulding, M. L.; Bedford, K.; Blumberg, A.; Cheng, R.; Swanson C. *ed.* Estuarine and coastal modeling III. Proceedings of the 3rd International Conference, Oak Brook, Illinois. New York, ASCE. Pp. 522–535.

Roig, L. C.; King, I. P. 1992: Continuum model for flows in emergent marsh vegetation. *In*: Spaulding, M. L.; Bedford, K.; Blumberg, A.; Cheng R.; Swanson, C. *ed.* Estuarine and coastal modeling. Proceedings of the 2nd International Conference, Tampa, Florida. New York, ASCE. Pp. 268–279.

Signell, R. P.; Geyer, W. R. 1990: Numerical simulation of tidal dispersion around a coastal headland. *In*: Cheng, R. T. *ed.* Residual currents and long-term transport. *Coastal and estuarine studies 38*. New York, Springer-Verlag. Pp. 210–222.

Simpson, J. H.; Hunter, J. R. 1974: Fronts in the Irish Sea. *Nature 250*: 404–406.

Speer, P. E.; Aubrey, D. G. 1985: A study of non-linear tidal propagation in shallow inlet/estuarine systems, Part II: Theory. *Estuarine, coastal and shelf science 21*: 207–224.

Thrush, S. F.; Pridmore, R. D.; Bell, R. G.; Cummings, V. J.; Dayton, P. K.; Ford, R.; Grant, J.; Green, M. O.; Hewitt, J. E.; Hines, A. H.; Hume, T. M.; Lawrie, S. M.; Legendre, P.; McArdle, B. H.; Morrisey, D. J.; Schneider, D. C.; Turner, S. J.; Walters, R. A.; Whitlatch, R. B.; Wilkinson, M. R. 1997: The sandflat habitat: scaling from experiments to conclusions. *Journal of experimental marine biology & ecology 216(1–2)*: 1–10.

Thrush, S. F.; Pridmore, R. D.; Hewitt, J. E.; Cummings, V. J. 1994: Impacts on soft-sediment macrofauna: the effects of spatial variation on temporal trends. *Ecological applications 4*: 31–41.

Tonkin & Taylor Ltd 1986: Manukau Harbour resources study, Volume I. *Report 6678*. A report to the Manukau Harbour Maritime Planning Authority. 171 p.

Vant, W. N. 1991: Underwater light in the northern Manukau Harbour, New Zealand. *Estuarine, coastal and shelf science 33*: 291–307.

Vant, W. N.; Williams, B. L. 1992: Residence times of Manukau Harbour, New Zealand. *New Zealand journal of marine and freshwater research 26*: 393–404.

Walters, R. A. 1987: A model for tides and currents in the English Channel and southern North Sea. *Advances in water resources 10*: 138–148.

Williamson, R. B.; van Dam, L. F.; Bell, R. G.; Green, M. O.; Kim, J. P. 1996: Heavy metal and suspended sediment fluxes from a contaminated, intertidal inlet (Manukau Harbour, New Zealand). *Marine pollution bulletin 32(11)*: 812–822.

APPENDIX 1

Model calibration amd performance

Calibration and verification

Calibration of the model was achieved by simulating the dominant M_2 tide where the open-boundary water elevation at time t was computed as:

$$\eta(t) = f_i A_i Cos(\omega_i t - g_i + E_i) \quad (3)$$

where A_i, g_i, ω_i, f_i, and E_i are respectively the amplitude, phase lag, angular frequency, nodal modulation factor and equilibrium argument of the ith tidal constituent, in this instance the M_2 (Walters 1987). The few historic measurements available over a wide swath along the north-western coast (Heath et al. 1977) all indicated that M_2 phases are clustered around 289°. The nearest node in the CSU world ocean tidal model (Egbert et al. 1994), 45 km offshore from Manukau Harbour, yielded an M_2 amplitude and phase of 109 cm and 268° (relative to NZST). To match the observed M_2 tide at the harbour entrance (Paratutae Island), the optimum values of M_2 amplitude and phase on the open-sea boundary (Fig. 2) were found to be 110 cm and 276.5° (or 4.5 ahead of Paratutae), which compare favourably with the CSU model results. The spatial distribution of the friction coefficient (Chezy C), which yielded the best overall match with water level and current velocity field data, was $C = 64$ $m^{0.5}$ s^{-1} over most of Manukau Harbour, except for the Papakura Channel, the ebb-tide delta and offshore waters beyond the entrance, where $C = 54$ $m^{0.5}$ s^{-1}. These Chezy values are within the range of other model studies (e.g., Dronkers 1964). The primary calibration of the tidal model was based on matching M_2 tide heights at eight harbour sites (Table 4). The comparison between observed and model tide elevations for Onehunga Wharf is shown in Fig. 10A (the most distant site from the entrance). The secondary calibration step involved comparing the simulated M_2 velocity components with available field data, mainly Papakura Channel (Sites 4, 5) and Mangere Inlet near Onehunga Wharf (Site 8). At these sites, model peak-ebb speeds were different to measured values by −8, −14, and −12% respectively, whereas for model peak-flood speeds, the differences were −10, +13, and −12%. The differences in peak-velocity phases were within 0.5 h. Although model velocities at these sites were mostly lower than measured values, the overall match is reasonable considering that the single-point current measurements have been scaled to an equivalent velocity at 0.4 of the depth above the bed and then compared to depth-averaged results from the nearest mesh node in the model.

The spring-tide model run, was used to verify the performance of the calibrated tidal-model, by freezing all model parameters such as the friction and eddy viscosity coefficients. For the offshore open boundary conditions, actual spring-tide water levels from the harbour entrance were transformed by the same phase difference and amplitude factor used in the calibration runs. The resulting match between the observed and

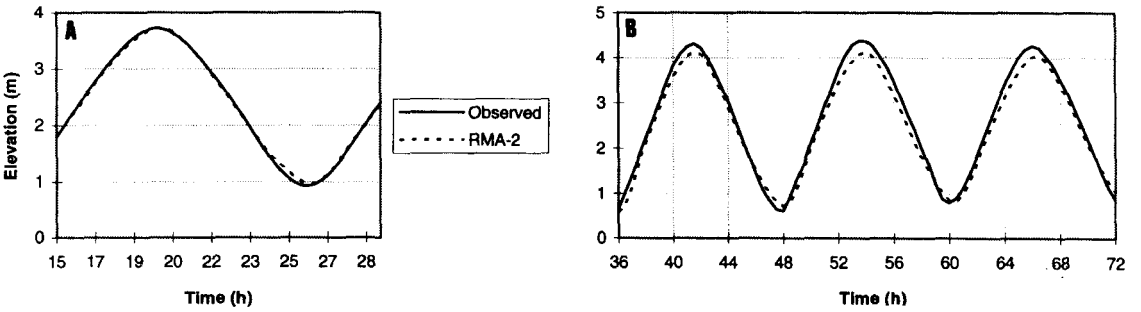

Fig. 10 Water level time series at Onehunga Wharf, New Zealand, comparing observed with modelled data for the: **A**, M_2 calibration run; and **B**, spring-tide verification run.

model water levels at Onehunga Wharf is shown in Fig. 10B. The simulated water level around high water for the middle cycle is somewhat lower (–0.19 m) than the observed spring high water at 53.5 h and similarly on the following ebb tide (partly because of set-up caused by a south-westerly wind peaking at 14 m s^{-1}), but otherwise the match at the low waters and the tide phasing is reasonable. A closer match was obtained at both other sites (Sites 2, 5) where concurrent observations were available. The comparisons between observed and simulated tidal elevations and velocities are reasonable enough to conclude that the tidal model produces reliable results.

Tidal model evaluation

The tidal model was evaluated mainly by comparing M_2 model results with observations from eight sites around Manukau Harbour, which were mainly short-term deployments of c. 1 month (Table 4). Discrepancies between model results and field observations are the result of both uncertainties in the observed harmonics (Foreman & Walters 1990; Foreman et al. 1995) and inaccuracies in the model formulation and application. Most of the observed records were no more then 1 month, so to reduce inaccuracies data measured during concurrent time periods was used wherever possible to optimise consistency. Inaccuracies are also present with the model, particularly in the way it is applied, such as the schematisation of the basin bathymetry and friction factor and in the instance of the M_2 simulation, interactions via the non-linear friction term with other Group 1 and 2 constituents are neglected. In particular for the Manukau Harbour, further refinements of the spatial distribution of the bed-friction coefficient and the finite-element mesh may be needed in the future, especially to redress the paucity of bathymetric data on the intertidal banks and southern inlets and improve resolution in the narrower channels. This should be complemented with longer term (> 1 month) field observations, to improve the match between observed and model simulations. Provided the finite-element mesh is carefully designed by aligning element boundaries with isobaths on intertidal areas, the application of the RMA-2 model described in this paper has demonstrated that finite-element models are capable of reliable simulation of estuarine hydrodynamics in harbours with extensive intertidal sandflats.